4 Modeling Intracellular Calcium Dynamics

Erik De Schutter

In this chapter we use the methods developed in chapter 3 to model calcium dynamics inside neurons. A wide range of applications are covered, from simple phenomenological models used to drive the activation of calcium-gated channels to highly detailed modeling of events in a spine. Simulating calcium dynamics can be computationally costly and even for extensively studied cases, important parameters are not known (Neher, 1998); therefore it is quite important to choose the right level of complexity of model. We only consider the cytoplasmic calcium concentration C_i and keep the extracellular concentration C_o constant because changes of the latter are not thought to be relevant under in vivo conditions. We will first introduce how to model the different processes affecting the cytoplasmic calcium concentration and then consider a number of typical modeling cases.

4.1 Calcium Sources and Sinks

The free cytoplasmic calcium concentration C_i is the end result of the interaction of many processes, each of which needs to be described by its own set of equations in a complete model. Recent reviews of the biochemical properties of these processes can be found in Sabatini et al. (2001), Augustine et al. (2003), Berridge et al. (2003), and Hartmann and Konnerth (2005). Neuroscientists should realize that the literature on modeling calcium dynamics is vast and extends well beyond the neuroscience domain, with many interesting contributions from modeling the heart, muscles, and pancreatic beta cells.

Calcium Influx

Calcium can flow into the cytoplasm from two sources: through membrane channels or by release from internal stores. The second source is considered later.

Because of the huge calcium gradient across the cell membrane, calcium currents are strongly rectifying (Hille, 2001). Therefore one should always use the Goldman-

Hodgkin-Katz equation (GHK; equations 5.12–5.13 in chapter 5) to compute the current I_{Ca}. This will be more accurate than a linear ohmic current because, for example, the calcium current reversal predicted by the Nernst potential is quite unphysiological.

The change in a concentration that is due to ion entry through a membrane channel caused by an ion current I_{Ca} (chapter 5) is given by

$$\frac{dC_i}{dt} = -\frac{I_{Ca}(t)}{zFv}, \tag{4.1}$$

where z is the charge of the ion (+2 in the case of calcium), F is the Faraday constant (96,489 $C \cdot mol^{-1}$), and v is the volume into which the flux occurs. An important parameter determining the rise and decay times of concentration changes caused by calcium currents is the surface-to-volume ratio (Cornelisse et al., 2007). The calcium influx scales with membrane surface as do the membrane pumps, but the effect of most removal systems like buffers and diffusion is related to the volume. Structures with a small volume (high surface-to-volume ratio) like spines and thin dendrites, will therefore, for the same density of calcium channels, show higher-amplitude changes that rise and decay faster than structures with high volumes, like a proximal dendrite.

For voltage-gated channels, usually the complete current is used to compute the calcium influx, but for many synaptic channels, the current is carried by a mixture of ions (chapter 6, section 1) and therefore the specific calcium component of the synaptic current is needed. This is most relevant for models that simulate calcium influx through NMDA and through some AMPA receptor channels (Burnashev, 1998) to induce synaptic plasticity (Holmes and Levy, 1990). The fractional calcium current, which expresses the relative charge carried by calcium at a given voltage, is in the range of 8–12% for NMDA channels (Burnashev, 1998; Sobczyk and Svoboda, 2007). This fraction is variable and can therefore not be directly applied to the synaptic current; this would also cause a reversal of the calcium current at the reversal potential of the synaptic channel (approximately 0 mV). Instead, one needs to compute the GHK equation for the calcium current through the synaptic channel and scale it by the time-varying synaptic conductance g_{syn} (Mayer and Westbrook, 1987; Badoual et al., 2006):

$$I_{CaS} = \bar{P}_{Ca} \frac{g_{syn}(t)}{\bar{g}_{syn}} G(V, Ca_o, Ca_i), \tag{4.2}$$

where $\bar{P}_{Ca}$ is scaled to obtain the correct fraction of current at the reference voltage and $G(V, Ca_o, Ca_i)$ is the GHK current equation (equation 5.13).

Calcium Removal

The free cytoplasmic calcium at rest is very low (around 50 nM) because most of the calcium is bound to buffers (see later) or removed effectively by Na^+-Ca^{2+} exchangers and ATP-driven pumps. Pumps are present on both the plasma membrane and the membrane of several organelles, with endoplasmic reticulum (Sabatini et al., 2002) and mitochondria (Friel, 2000) being the largest calcium sinks. Removal has a strong effect on calcium dynamics and in the case of small structures like spines it may even dominate the decay time of calcium signals (Sabatini et al., 2002). In general, neuron models have not been very sophisticated in simulating membrane transporters compared with the detailed modeling that is common for cardiac cells (e.g., DiFrancesco and Noble, 1985; and more recently the Kyoto model, which contains four membrane transporters and several leak currents; Takeuchi et al., 2006).

The Na^+-Ca^{2+} exchanger (Blaustein and Lederer, 1999; Dipolo and Beaugé, 2006) is a low-affinity high-throughput system that uses the sodium gradient to remove calcium, with a stoichometry of probably 3:1. The classic model by DiFrancesco and Noble (1985):

$$I_{NaCa} = k_{NaCa}([Ca^{2+}]_o[Na^+]_i^3 e^{\gamma FV/RT} - [Ca^{2+}]_i[Na^+]_o^3 e^{(\gamma-1)FV/RT})/$$
$$(1 + 0.001([Ca^{2+}]_i[Na^+]_o^3 + [Ca^{2+}]_o[Na^+]_i^3)) \tag{4.3}$$

is still often used, with k_{NaCa} the maximum rate (in units of A mM^{-4}, taken proportional to the membrane surface), $[\ ]_o$ and $[\ ]_i$ representing outside and inside concentrations, respectively, and the partition parameter γ representing the fractional position within the membrane of the voltage-sensitive energy barrier (Hille, 2001), usually taken to be 0.38. A disadvantage of this simple model is that it does not represent the affinities of the calcium and sodium binding sites, which are incorporated into more modern models (Cortassa et al., 2003; Takeuchi et al., 2006). Since the Na^+-Ca^{2+} exchangers come in several molecular forms (Philipson and Nicoll, 2000), one can expect future models to be based on the kinetics of specific gene products. Usually only the exchange over the plasma membrane is modeled, but in reality exchange also occurs with internal organelles like mitochondria (Cortassa et al., 2003).

Equation (4.3) is formulated as a current and emphasizes, therefore, an important property of exchangers and pumps: they are electrogenic. In the case of the Na^+-Ca^{2+} exchanger, this results in an inward current ($z = -1$) when $[Ca^{2+}]_i$ becomes high, although this depends on the exact stoichiometry of the exchange (Blaustein and Lederer, 1999).

The Ca-ATPase pumps are present both on the plasma membrane (PMCA family) and on the sarco/endoplasmic reticulum (SERCA family) (Strehler and Treiman, 2004). These high-affinity, low-capacity pumps are often modeled with a simple Hill (1910) equation:

$$\frac{dC}{dt} = V_{\max} \frac{C^n}{K_d + C^n}, \tag{4.4}$$

with $V_{\max}$ as the maximum pump rate (units of moles per second taken proportional to the membrane surface), K_d the dissociation constant, and n the Hill constant (a measure of cooperativity between the binding sites). For $n = 1$, equation (4.4) reduces to the Michaelis-Menten function (chapter 3, section 2; Michaelis and Menten, 1913). Kinetic models for the different isoforms of SERCA pumps are becoming available (Dode et al., 2002; Yano et al., 2004); these models also include the inhibitory effect of the calcium store concentration on the pumps (Burdakov et al., 2005). Further elucidation of the structural basis of calcium movement by these pumps (Olesen et al., 2007) may lead to a new generation of kinetic models.

The PMCA pump generates an outward current ($z = 2$) and therefore it will counteract the current caused by the Na^+-Ca^{2+} exchanger. The net electrogenic effect of the pumps and exchangers is usually neglected in neural simulations but can nevertheless reach about 1% of the amplitude of I_{Ca} and modulate it significantly (De Schutter and Smolen, 1998).

One problem in using simple models of the exchanger and pumps, as in equations (4.3) and (4.4), is that they may drive calcium below its resting concentration. A common solution to this problem is to use a small leak from the endoplasmic reticulum, which is calibrated to give a stable resting concentration (Schmidt et al., 2003), but this may require rather large leak currents. Shannon et al. (2000) have proposed a more physiological model that includes the reverse mode of the SERCA pumps.

Calcium Release

Gated calcium release from internal stores in endoplasmic or sarcoplasmic reticulum can cause large changes in the internal calcium concentration. Calcium release is best known for its important role in the generation of calcium oscillations and calcium waves (Berridge et al., 2003; Fiacco and McCarthy, 2006), but it also contributes to the induction of synaptic plasticity in many systems (Bardo et al., 2006). Two important receptor channel types have been identified: inositol triphosphate (IP_3) (Taylor and Laude, 2002) and ryanodine (Fill and Copello, 2002) receptors, both of which have multiple subtypes. The expression of these receptors and their distribution are cell specific.

Calcium release is usually modeled as a ligand-dependent flux along the concentration gradient:

$$\frac{dC_i}{dt} = V_R f_o (C_s - C_i), \tag{4.5}$$

where V_R represents the maximum rate of release, f_o the fraction of open channels, and C_s the calcium concentration in the stores. Phenomenological models often use

a Hill function (equation 4.4) to relate f_o to the ligand concentration and equation (4.5) can then be solved as a simple ODE (chapter 1, section 6). For both receptor types, more complex Markov gating models (chapter 5, section 5) are available.

Another issue is how to model the calcium store concentration C_s. This concentration is quite high, 100–800 μM (Burdakov et al., 2005), and strongly buffered. The dynamics of calcium stores can influence the overall changes in cytoplasmic calcium concentration to a large degree; for example, in some models of calcium oscillations, the calcium release ends because of depletion of the store (Goldbeter et al., 1990). Recently it was confirmed that calcium release may indeed lead to highly localized decreases of the calcium store concentration (Brochet et al., 2005).

The IP_3 receptor is activated by both calcium and IP_3. The source of the latter in neurons is activation of membrane-bound G-protein-linked receptors like the metabotropic glutamate receptors (mGluR) (Coutinho and Knöpfel, 2002). The calcium influx caused by IP_3 receptors has been modeled extensively to simulate calcium oscillations, first with phenomenological models (Goldbeter et al., 1990) and then with simple binding models (De Young and Keizer, 1992). The latter was the first model to include the dual action of calcium. At low concentrations it activates the IP_3 receptor, whereas higher calcium concentrations inactivate it (Taylor and Laude, 2002). Although this model is still extensively used, including a simplified version (Li and Rinzel, 1994), it has been outdated by the avalanche of recent molecular and biochemical data. Several more sophisticated models have been proposed recently (Doi et al., 2005) and have been reviewed by Sneyd and Falcke (2005). In addition to modeling the receptor, IP_3 metabolism needs to be simulated also. In many simulations this has been approximated as a pulse combined with a linear decay, but more detailed kinetic schemes have been proposed (Bhalla and Iyengar, 1999).

The molecular mechanisms underlying ryanodine receptor activation are less well known (Fill and Copello, 2002). It is suspected that ryanodine receptors are activated by a specific, unidentified signaling molecule, but they are best known as the receptors of calcium-induced calcium release (CICR) because their opening is strongly facilitated by increases of C_i and of C_s. Again, both phenomenological (Keizer and Levine, 1996) and complex gating models (Zahradnik et al., 2005) have been proposed.

Calcium Buffering

Calcium buffering can be a source or a sink of calcium, depending on the balance between bound and free calcium. In fact, most of the cytoplasmic calcium is not free but is bound to different proteins. Neurons express a particular class of proteins called calcium buffers that are characterized by the presence of multiple EF-hand calcium-binding domains (Lewit-Bentley and Rety, 2000), for example, calbindin, calmodulin, and parvalbumin. The different calcium binding sites on these buffer

proteins will usually also have different rate constants and show cooperativity (Faas et al., 2007), but such complexity is often ignored (however, see W. R. Holmes, 2000; Schmidt et al., 2003; Naoki et al., 2005; Means et al., 2006; and Kubota et al., 2008 for models using binding site-specific rate constants). Under these simplifying conditions, the interaction of calcium with buffers is reduced to a second-order reversible reaction (chapter 3, section 2):

$$Ca^{2+} + B \underset{k_b}{\overset{k_f}{\rightleftarrows}} CaB, \tag{4.6}$$

with a forward rate constant k_f and a backward rate constant k_b, which are related to the dissociation constant K_d of the buffer as $K_d = k_b/k_f$. An important issue is whether the buffer is mobile. Several experimentalists have the impression that cytoplasmic buffers are immobile because little or no washout is observed (Helmchen et al., 1996; Sabatini et al., 2002). In fact, however, most buffers have diffusion constants D_B in the range of 20–50 $\mu m^2/s$ (Schmidt et al., 2003), although the value for calmodulin is unclear (Naoki et al., 2005). Fractions of these buffers may be bound to cytoskeleton, but the majority of the molecules remain mobile (Schmidt et al., 2005). So for a complete model of calcium buffering, one requires for each buffer four parameters: the rate constants k_f and k_b, the diffusion constant D_B, and the total buffer concentration $[B]_T$ (the sum of $[B]$ and $[CaB]$). The first three parameters are known for the most common calcium buffers (e.g., Schmidt et al., 2003 for parvalbumin and calbindin and Means et al., 2006 and Tadross et al., 2008 for calmodulin or calreticulin) but $[B]_T$ is neuron specific and often a free parameter. A useful experimental value to constrain $[B]_T$ is the buffer capacity κ of the neuron, the fractional amount of bound over free calcium:

$$\kappa = \frac{d[CaB]}{d[Ca^{2+}]}. \tag{4.7}$$

Buffer capacity can be measured experimentally (Maravall et al., 2000) and ranges from 20 to 200 in most neurons (Neher, 1998; Sabatini et al., 2002) and up to 2,000 in Purkinje cells (Hartmann and Konnerth, 2005). Notice that κ may vary locally within neurons (Neher, 1998; Sabatini et al., 2002). Buffer capacity is related to the total buffer concentration for buffers with a low affinity (high K_d):

$$\kappa \approx \frac{[B]_T}{K_d} \quad \text{if } [Ca^{2+}] \ll K_d. \tag{4.8}$$

Calcium stores have high concentrations of specific buffers like calsequestrin and calreticulin, which have large numbers of calcium-binding sites but low affinity (Beard et al., 2004).

4.2 Calcium Diffusion

Diffusion of calcium, or of other signaling molecules like IP_3, and of buffer molecules, can be simulated with any of the methods described in chapter 3, section 5. The diffusion constant D should be based on measurements in cytoplasm because this has a much higher viscosity than water; for example, D_{Ca} for cytoplasm is 2×10^{-6} cm^2 s^{-1}, which is three times slower than in water (Albritton et al., 1992). Note that the value for D_{Ca} used in the simulations may be very different from the experimentally observed apparent diffusion constant D_{app}, because many factors may affect the measured D_{app} (section 4.3 and Santamaria et al., 2006; Wagner and Keizer, 1994).

Numerical Solution and Dimensionality

In general, solving the diffusion equation is an expensive operation. We focus here only on deterministic solutions, but similar issues apply when stochastic methods are used (chapter 3, section 5). Numerical accuracy will require the use of smaller discretization steps both in the spatial (submicrometer) (Carnevale and Rosenthal, 1992) and time (about 1 μs) domains compared with the voltage equation (11.1), resulting in calculations that are several orders of magnitude slower (De Schutter and Smolen, 1998). For one- and two-dimensional diffusion, implicit methods can be used; explicit methods require even smaller time steps. The Crank-Nicholson method works quite well for the tridiagonal matrix describing a one-dimensional case (Fletcher, 1991; Press et al., 2007) and can be used in two dimensions with the alternating direction implicit (ADI) method (Press et al., 2007; see W. R. Holmes, 1995 for a neuroscience implementation). A specialized ADI implementation for modeling calcium dynamics in one to three dimensions is the program CalC (see the software appendix; Matveev et al., 2002). Deterministic modeling of three-dimensional diffusion usually employs finite-volume approaches based on slower, iterative solution methods (Ferziger and Peric, 2001).

Traditionally, many neural models have limited themselves to one-dimensional diffusion in modeling spines (W. R. Holmes and Levy, 1990; W. R. Holmes, 2000) or activation of membrane channels (De Schutter and Smolen, 1998; Yamada et al., 1998) because such models are relatively easy to solve. Of course this simplification does not allow accurate simulation of highly local phenomena like calcium nanodomains (Berridge, 2006; see section 3), which need a full 3-D simulation. Even in cases where only diffusion over long distances is of interest, ignoring some spatial dimensions may come at a risk. For example, a detailed 2-D simulation of IP_3 diffusion in Purkinje cell spiny dendrites (Hernjak et al., 2005) did not report the experimentally observed anomalous diffusion of IP_3 caused by trapping in spines (Santamaria et al., 2006). The discrepancy is explained by the difference in spine

density between 2-D and 3-D models of the spiny dendrite, which strongly influences the occurrence of anomalous diffusion (Santamaria et al., 2006). For simple geometric reasons, 2-D models can never approach the real spine density of Purkinje cells.

Electrodiffusion

Treating the computation of changes in membrane potential (chapter 10) and the diffusion of ions as separate processes is a simplification because the membrane electric field can exert an effect on charged molecules. Similarly, the axial current computed by the cable equation (10.2) is in reality caused by the drift of ions. Proper treatment of this interaction requires the use of the Nernst-Planck equation (Jack et al., 1975), which is rather cumbersome. Qian and Sejnowski (1989) have argued that in thin dendrites (0.1 μm) application of the full electrodiffusion equation is required to track fast changes in ionic concentration, and they proposed a modified cable equation. Most of the effects they describe, however, can already be simulated by the proper use of the Nernst or Goldman-Hodgkin-Katz equations (chapter 5, section 3) to track changes in the ion equilibrium potential.

Moreover, using the electrodiffusion equation forces the modeler to consider many cellular details that are normally ignored and that are often poorly characterized. Examples include the actual charge carriers in the cytoplasm, which may include small organic molecules like phosphates (De Schutter and Smolen, 1998; Lopreore et al., 2008), and the variable membrane potential of intracellular organelles (Shemer et al., 2008; Wikström et al., 1997; Yamashita et al., 2006). Since thermal velocities of molecules (causing the Brownian motion) are almost an order of magnitude larger than the drift velocities in an electrical field (Hille, 2001), it is unlikely that simulating the full electrodiffusion equation appreciably changes simulation results compared with the standard methods derived from the cable equation (Koch, 1999). Comparisons of a simulation of action potential generation at the node of Ranvier by the cable equation and by an electrodiffusion model (Lopreore et al., 2008) showed small differences in the width of the action potential, but at present it is not clear whether this prediction is physiologically relevant.

4.3 How to Choose the Right Approach to Modeling Calcium

It is difficult to model calcium accurately because most simulation approaches are really gross simplifications of reality. Calcium entry, whether through the plasma membrane or from internal sources, is a highly local process, occurring in nanodomains (below a single channel) and microdomains (below a cluster of channels; Augustine et al., 2003; Berridge, 2006). Influx from a single channel into the cytosol typically consists of about a thousand ions and causes a rise to a concentration of several hundred micromolars in a plume with dimensions of ~10 nm. This plume has been given

different names, depending on the source of calcium: sparks, puffs, sparklets, and scintillas (Berridge, 2006). Correct modeling of calcium concentrations in a nano- or microdomain remains a challenge because of the strong gradients, requiring finite-volume or stochastic approaches on very fine grids (Aharon et al., 1994; Meinrenken et al., 2002; Shahrezaei and Delaney, 2004).

Since some calcium sensors, such as Ca^{2+}-activated K^+ channels, sample concentration in these microdomains (Goldberg and Wilson, 2005; Zhuge et al., 2002; Fakler and Adelman, 2008), an accurate simulation would require a detailed, computationally expensive simulation. This is almost never feasible or desired and instead, modelers use simplified models of calcium dynamics. The question then becomes: What is the proper simplification to use?

Simple Calcium Pools to Simulate Channel Activation by Calcium

Compartmental neuron models (chapter 11, section 1) often need to compute calcium concentration to activate Ca^{2+}-dependent channels (chapter 5) in the plasma membrane. Since the calcium concentration itself is usually not of primary interest, the model can be highly simplified. The most commonly used model is the exponentially decaying Ca^{2+} pool (Traub and Llinás, 1977):

$$\frac{dC_i}{dt} = -\frac{I_{Ca}(t)}{2Fv} - \beta(C_i - C_{min}). \tag{4.9}$$

This model contains a biophysical component, the influx (compare with equation 4.1), and a phenomenological one, the removal of calcium. The influx is scaled by a volume v. Although it may seem that v is fixed by the size of the electrical compartment, it is in practice a free parameter because for large compartments it makes more sense to consider the calcium concentration only in the submembrane region, where it is sampled by the Ca^{2+}-activated channels. Therefore v is often taken as the volume of a submembrane shell about 0.2 μm deep (De Schutter and Bower, 1994a), thinner shells causing steeper changes in calcium concentration. The removal of calcium is governed by the parameter β, which lumps together the effects of buffers, pumps, and diffusion. β is the inverse of the time constant of exponential decay and therefore this parameter will determine how fast calcium returns to the resting concentration C_{min}. A wide range of values are used for this parameter; decay time constants ($1/\beta$) range from 0.1 ms (De Schutter and Bower, 1994a) to 50 ms (Traub and Llinás, 1977). Fast decay time constants combined with thin submembrane shells make the computed calcium concentration track calcium influx closely, which is a reasonable approximation of the changes in microdomain concentration (Sherman et al., 1990) and can be used to activate BK-type Ca^{2+}-activated potassium channels (Zhuge et al., 2002; Fakler and Adelman, 2008).

One problem with the calcium pool is that it reduces the calcium dynamics to a single time constant. If, for example, multiple types of Ca^{2+}-activated K^+ channels need to be simulated, this may cause a problem because these typically show different dynamics. SK-type Ca^{2+}-activated potassium channels activate slower than BK channels and the difference is attributed to the indirect activation by calcium (Fakler and Adelman, 2008). A simple and effective solution is to use two or more calcium pools with different values for β (Tegnér and Grillner, 1999). This can be implemented in different ways. One can distribute the calcium influx over the pools or one can attribute specific pools to different sources of calcium (Tegnér and Grillner, 1999). Although this approach is attractive, it increases the number of purely phenomenological parameters in the model. Therefore, especially if the data are available, one should instead consider a more detailed calcium buffering model in which the different affinities of the Ca^{2+}-activated channels make them sense varying time constants of the system (see the following discussion).

Calcium Buffering in a Single Compartment

If the binding properties of the intrinsic calcium buffers are known, as is now the case for an increasing number of neurons (Cornelisse et al., 2007; Schmidt et al., 2003), it is more realistic to model a system with calcium buffers and pumps at only a little added computational cost (figure 4.1). Each additional buffer introduces two new

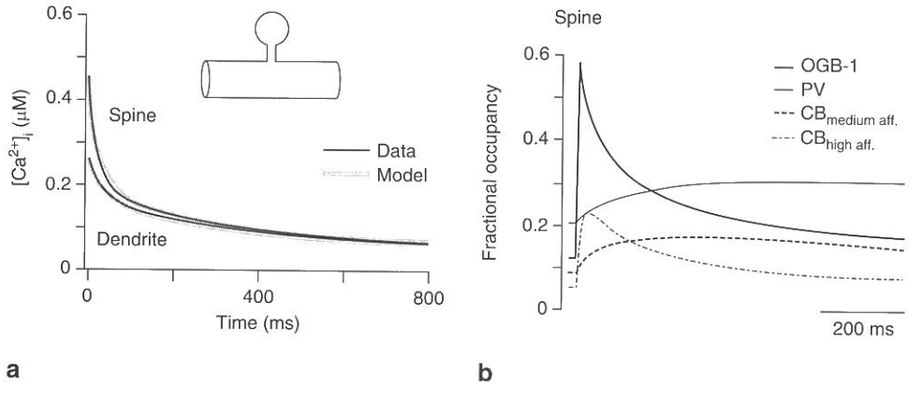

Figure 4.1
Simulation of calcium decay kinetics in a Purkinje cell spine. The model is parametrized based on comparing calcium imaging data in normal and transgenic mice and includes three diffusible buffers: the calcium dye (OGB-1), calbindin (CB, two binding sites), and parvalbumin (PV). Panel a shows that the model replicates well the biphasic calcium decay observed experimentally in both spine and dendrite. Panel b shows the calcium binding of the different buffers in the spine. It indicates that the biphasic decay is caused by the different binding kinetics of the two intrinsic buffers and that the measurements in spines suffer from saturation of the calcium dye. (Modified with permission from Schmidt et al. 2003.)

time constants to the system, causing more complex calcium dynamics in the model. The forward rate of the buffer will be critical in determining the maximum rise in calcium concentration. An exception is buffer saturation, i.e., when most of the buffer calcium binding sites become occupied, because then the system reverts to the unbuffered behavior (Bormann et al., 2001).

Removal of calcium can be modeled as a single high-rate calcium pump. Such a single-compartment system ignores the effects of diffusion, but this simplification is justified in some structures, such as a dendritic spine (Sabatini et al., 2002). If one adds a few more molecular features to such a simulation, e.g., calcium release from intracellular stores, it becomes a valuable tool in a systems biology approach to simulate signaling pathways involved in the induction of synaptic plasticity (Doi et al., 2005).

For larger structures where calcium influx across the cell membrane is the primary source, diffusion toward the center becomes more important (Yamada et al., 1998). In principle, one could approximate the removal that is due to diffusion phenomenologically (equation 4.9) and use this single-compartment buffering approach to model the calcium concentrations needed to activate potassium channels, but this approach has not yet been tested in large compartmental models (chapter 11, section 1).

Buffered Calcium 1-D Diffusion to Model Calcium Imaging Data

A more realistic approach is to include 1-D diffusion of calcium and the mobile buffers into the model, but this steeply increases the computational cost. Such systems have been investigated extensively, using both analytical (Naraghi and Neher, 1997; Wagner and Keizer, 1994; Zador and Koch, 1994) and modeling (Nowycky and Pinter, 1993) approaches. An important concept introduced by these studies is the apparent diffusion constant for buffered calcium diffusion, D_{app}:

$$D_{app} = \frac{1}{1+\kappa} D_{Ca} + \kappa D_B, \tag{4.10}$$

where the buffer capacity κ was defined in equations (4.7) and (4.8). D_{app} is a convenient way to describe how binding to buffers affects calcium diffusion. However, the simplification is valid only for the steady state in the presence of unsaturated buffers with a fast forward rate (Wagner and Keizer, 1994) and therefore in most models a full simulation is warranted (Bormann et al., 2001). In the presence of an immobile buffer ($D_B = 0$), equation (4.10) predicts a slowing down of the calcium diffusion because of calcium binding to the buffer. This effect steeply limits the spatial extent to which calcium can affect chemical reactions in the neuron compared with other signaling molecules with similar diffusion constants that are not buffered, such as IP_3 (Kasai and Petersen, 1994; Santamaria et al., 2006). It is interesting that calcium

seems to diffuse effectively over long distances, although slowly, in the endoplasmic reticulum (Choi et al., 2006; Mogami et al., 1997) despite its assumed high buffer capacity.

The mobility of buffers ($D_B > 0$ in equation 4.10) can reverse this situation because they may increase D_{app} by shuttling calcium from high concentration regions (where they bind calcium) to low concentration regions (where they unbind it) (Bormann et al., 2001; Wagner and Keizer, 1994).

This is one of the problems that calcium dyes introduce. Most calcium dyes act as mobile buffers and may modify the calcium dynamics being observed by changing both buffer capacity and apparent diffusion (A. Takahashi et al., 1999). One solution is to use low-affinity dyes only, but this excludes measuring small changes in concentration from that at rest (S. S. Wang et al., 2000). An alternative is to use modeling methods to estimate the error (H. Blumenfeld et al., 1992; Cornelisse et al., 2007; Sala and Hernandez-Cruz, 1990). This can even be done with a spreadsheet (McHugh and Kenyon, 2004; http://www.medicine.nevada.edu/physio/docs/diffusion.htm). The basis of these models is 1-D buffered calcium diffusion in a spherical cell (Yamada et al., 1998), combined with a transfer function to compute the fluorescence from the concentrations of bound and unbound calcium dye (Grynkiewicz et al., 1985) and, possibly, a model of the filtering properties of the imaging equipment (H. Blumenfeld et al., 1992).

Buffered 1-D diffusion has also been used to simulate calcium transients in dendritic spines, where the spine is modeled using an FD approach (chapter 3, section 5) by stacking a set of thin cylinders on each other (W. R. Holmes and Levy, 1990; Zador et al., 1990). Although such simulations have provided useful insights, they are being replaced with more detailed 3-D models (Keller et al., 2008).

A Full 3-D Model to Simulate Calcium Signaling Pathways

This is the ne plus ultra in calcium modeling and the appropriate tool for modeling the effect of calcium nano- and microdomains. It is, however, not only challenging to compute these complex models, but also to design them. The number of molecular species simulated and the specification of parameters and boundary conditions make the development and tuning of these models as demanding as large compartmental models (chapter 11).

As a result, many recent examples simulate only a small part of a neuron, i.e., signaling events in a spine (Ichikawa, 2005; Keller et al., 2008) or calcium entry in a presynaptic terminal (Bennett et al., 2000; Meinrenken et al., 2002). It is interesting that stochastic simulation is being used extensively in neuroscience for such models, with MCell or STEPS (see the software appendix). This is quite different from the systems biology approaches, which focus more on the use of finite-element methods

in unstructured meshes to attempt to model signaling in large parts of reconstructed cells and organelles (Hernjak et al., 2005; Means et al., 2006).

Based on continuous improvements in calcium imaging techniques, combined with the increase in available computer speed and the rapid development of new software tools for 3-D simulation, we expect to see exciting new, detailed calcium models in the near future.